

MODELING DEFORMATION AND RECRYSTALLIZATION SHEAR TEXTURES IN OLIVINE

Javier Signorelli^a, Roland Loge^b, Raul Bolmaro^a, Andrea Tommasi^c

^a Instituto de Física Rosario, CONICET - Universidad Nacional de Rosario, Bv. 27 de Febrero 210 bis
- Rosario – Argentina. <http://www.ifir-conicet.gov.ar>

^b Centre de Mise en Forme des Matériaux (CEMEF), UMR CNRS 7635, Ecole des Mines de Paris,
B.P. 207, Sophia-Antipolis Cedex 06904, France. <http://www.cemef.mines-paristech.fr>

^c Laboratoire de Tectonophysique – UMR 5568 Place Eugene Bataillon, Montpellier, France.
<http://www.gm.univ-montp2.fr>

Keywords: Olivine, dynamic recrystallization, texture, continuity of lattice spin.

Abstract. Low-symmetry rock materials subject to simple shear have stable texture components characterized by pole figures showing a girdle aligned parallel to the macroscopic shear or lineation direction. Microscopic observations in olivine polycrystals indicate that the majority of the crystals in those stable orientations are highly elongated and possess rather high dislocation densities, suggesting that neither recrystallization nor grain growth alone have been the dominant phenomenon. To understand the link between active slip systems and texture development we use a self-consistent tangent polycrystal plasticity theory in conjunction with a deformation-based recrystallization model that balances nucleation and growth. An ‘ad hoc’ grain-to-grain interaction scheme is incorporated to take into account the short range interaction and high mechanical heterogeneities between grains as a consequence of olivine having only three easy slip systems: (010)[100], (001)[100], and (010)[001]. The proposed model couples pairs of neighbor crystals, where their plastic spins are taken as an average of the individual ones. That results in a nonlocal evolution equation, introducing continuity of the lattice rotation field, as a constraint at the grain boundary interface. In this first approach, the selection of crystal pairs is random and leaving uncoupled the mechanical response. In particular, the proposed model correctly predicts the asymptotical evolution of texture orientations towards a constant orientation parallel to the shear plane and smaller growth intensity. Soft orientations with large strain energy will grow preferentially, while hard orientations accumulate dislocations. The effect of the lattice rotation field continuity induces less severe Lattice Preferred Orientations (LPO), which is in better agreement with the experimental observations.

1 INTRODUCTION

Olivine is one of the most important geophysical materials in the study of the Earth's upper mantle behavior, i.e. it constitutes approximately 50-80% of its total mass (Bai et al., 1991). Olivine aggregates deform and develop Lattice Preferred Orientations (LPO) during convection having an important influence on the seismic anisotropy (Mainprice and Silver, 1993). Its rheology is therefore crucial for understanding both the lithosphere deformation and the mantle convection. Olivine presents an orthorhombic crystallographic symmetry which is highly anisotropic because the total number of slip systems is reduced, while CRSS values vary considerably from one system to another. A direct consequence of this plastic anisotropy is the development of strong LPO during deformation by dislocation creep leading to an anisotropic mechanical behavior at the polycrystal scale. Analysis of naturally and experimentally deformed upper mantle rocks allows the determination of the LPO patterns that may develop during plastic deformation. Correlations between strain, LPO intensity and strain paths in natural peridotites are not possible. Numerical models of LPO evolution of polycrystalline aggregates offer an insight into how LPO development is influenced by the micromechanical mechanisms. They also offer the possibility of predicting LPO, and thus the upper mantle anisotropy, associated with a specific flow process.

Zhang and Karato (1995), studied the effects of plastic flow by dislocation glide on the development of LPOs in olivine grains showing that, at large strains, the microscopic slip direction [100] and slip plane (010) are aligned parallel to the macroscopic shear direction and shear plane respectively, supporting the fact that the geometrical flow controls de LPO development. Nevertheless, in their work the authors only measured the large grains (due to techniques limitations), where presumably dynamic recrystallization take places. More recently, many authors have shown that recrystallization migration in olivine is found when strain exceeds a critical value (Zhang et al., 2000; Bystricky et al., 2000). In this sense, in order to simulate the deformation of the Earth's mantle it is necessary to include recrystallization into the proposed model. A variety of glide-based models: stress equilibrium models (Chastel et al., 1993); kinematic constraint (Ribe et al., 1991); self-consistent VPSC (Wenk et al., 1991), predicts that the LPO of initially isotropic aggregates align the a-axis of olivine crystals towards the elongated direction of the finite strain ellipsoid. Experimental evidence shows that these results are in agreement with the observations at small shear strains (Zhand and Karato, 1995). Kaminski et al. (2004), proposed a refined version of D-Rex model using a simplified theory for crystal rotation by plastic deformation and dynamic recrystallization, involving only a small number of parameters. Frequently, in models of dynamic recrystallization, the deformation of each crystal is used to estimate its dislocation density which itself drives the dynamic recrystallization. Wenk and Tome (1999), also presented and discussed the results of a deformation-based model for dynamic recrystallization implemented in conjunction with the VPSC model for predicting deformation texture in olivine deformed in simple shear to large strains.

Thorsteinsson (2002) studied the fabric development and macroscopic deformation by examining three effects: nearest-neighbor interaction among crystals, polygonization, and migration recrystallization. The author introduces the short interaction effects by arranging the crystals on a three-dimensional cubic grid and assigning six neighbors to each crystal. The strength of interaction can be controlled varying from no interaction (homogeneous stress) to a high interaction (heterogeneous stress). Recrystallization is described by an energy-based model, and the polygonization is formulated in terms of stress differences. The strength of the

interaction is modeled by defining a local softness parameter relating the stress acting on the central crystal and the Cauchy stress at the aggregate. The author concluded that the inclusion of the nearest-neighbor interaction change the rate of fabric development.

Recently, Mach et al. (2010) gave some theoretical basis for the assumptions of the co-rotation method to describe short-range interaction between the neighbor grains. These authors shown, based on an average theory of field dislocation mechanics, that a continuity condition on the constitutive velocity gradient results in the continuity on the lattice rotation field. This techniques have been used by Bolmaro et al. (2000) and Tomé et al. (2002) together with self-consistent models to simulate texture development in metals. More recently, Bolmaro et al. (2006) and Signorelli et al. (2006) used similar ideas coupled with finite elements to analyze recrystallization and grain fragmentation processes. The common feature of those works is the texture development simulation by accounting for continuity of the spin (CS) at grain boundary.

The purpose of this paper is to present a new model for fabric development that enforces the continuity of the lattice rotation field between the nearest-neighbor grains. We use a modified self-consistent viscoplastic approach (Lebensohn and Tomé, 1993) to include the continuity of the lattice rotation field (Mach et al., 2010). In order to simplify the implementation of the continuity constraint of lattice spin tensor, we take the idea of co-rotation or co-spin introduced by Bolmaro et al. (2000). This technique inforces that pairs of grains sharing an interface must keep constant the relative orientation (i.e. they must co-rotate). In this sense, this model should be seen as a first attempt to investigate the effects of including spin continuity in the development of texture, accumulation of energy and its further use in simple models of recrystallization. Simulations for simple shear tests in olivine are discussed and the results are compared with classical TGT - VPSC simulations. The proposed VPSC-CS extension is also tested in conjunction with a deformation-based recrystallization model.

2 VISCOPLASTIC CRYSTAL PLASTICITY

For the sake of simplicity we restrict the implementation to a viscoplastic formulation. As well as in metals, this is a common assumption in large strain plasticity of rocks where the elastic strains are at least two orders of magnitude less than the plastic contribution. Using a dot to indicate time derivation, the velocity gradient tensor is:

$$\mathbf{L} = \dot{\mathbf{F}}:\mathbf{F}^{-1} = \dot{\mathbf{R}}^*:\mathbf{R}^{*\text{T}} + \mathbf{R}^*:\mathbf{L}^p:\mathbf{R}^{*\text{T}} \quad (1)$$

In this expression, \mathbf{R}^* represents the crystallographic rotation, and \mathbf{F} corresponds to the effect of dislocation slip on the crystal deformation and $\mathbf{L}^p = \dot{\mathbf{F}}^p:\mathbf{F}^{p-1}$ is the plastic velocity gradient resulting from dislocation motion along specific planes and directions of the crystal. Potentially active slip systems are labeled with the superscript s :

$$\mathbf{L}^p = \sum_s (\mathbf{n}^s \otimes \mathbf{b}^s) \dot{\gamma}^s \quad (2)$$

The symmetric part of $\mathbf{n}^s \otimes \mathbf{b}^s$, \mathbf{m}^s , is the symmetric part of the Schmid orientation tensor of the system (s) defined by its normal to the glide plane \mathbf{n} and the Burgers vector \mathbf{b} :

$$\mathbf{m}^s = \frac{1}{2} (\mathbf{n}^s \otimes \mathbf{b}^s + \mathbf{n}^s \otimes \mathbf{b}^s) \quad (3)$$

Complementary, the screw-symmetric tensor associated with crystallographic spin is given by:

$$\mathbf{q}^s = \frac{1}{2}(\mathbf{n}^s \otimes \mathbf{b}^s - \mathbf{n}^s \otimes \mathbf{b}^s) \quad (4)$$

Here, $\dot{\gamma}^s$ represents dislocation slip rates that are derived from the stress tensor \mathbf{s} using a viscoplastic exponential law (Hutchinson, 1972):

$$\dot{\gamma}^s = \dot{\gamma}_0 \left(\frac{\mathbf{m}^s : \mathbf{S}}{\tau_c^s} \right)^{1/m} \text{sign}(\mathbf{m}^s : \mathbf{S}) \quad (5)$$

$\dot{\gamma}_0$ is the reference slip rate, m is the strain rate sensitivity exponent, and τ_c^s is the critical resolved shear stress on the slip system labeled s . Eq (3) and eq (4) allow us to decompose the velocity gradient into a strain rate and a rotation rate:

$$\mathbf{L}_o = \mathbf{D}_o + \mathbf{W}_o; \quad \mathbf{L} = \mathbf{D} + \mathbf{W} \quad (6)$$

where the subscript (o) indicates initial crystal axes. The distortion rate tensor \mathbf{D} and the rotation rate tensor \mathbf{W} can be obtained by evaluating the symmetric and screw-symmetric part of equation (1) respectively:

$$\mathbf{D} = \mathbf{R}^* : \mathbf{D}^p : \mathbf{R}^{*T} \quad (7)$$

$$\mathbf{W} = \mathbf{\Omega} + \mathbf{R}^* : \mathbf{W}^p : \mathbf{R}^{*T} \quad (8)$$

where the lattice spin tensor is defined as $\mathbf{\Omega} \equiv \dot{\mathbf{R}}^* : \mathbf{R}^{*T}$. The evolution equation for \mathbf{R}^* consists in its update by using the exponential map (Simo and Vu-Quoc, 1985):

$$\dot{\mathbf{R}}^* = \mathbf{\Omega} : \mathbf{R}^{*T}; \quad {}^{t+\Delta t}\mathbf{R}^* = \exp(\mathbf{\Omega}) : {}^t\mathbf{R}^* \quad (9)$$

Rearrangement of the equation for the screw-symmetric part of the velocity gradient (8) gives $\mathbf{\Omega} = \mathbf{W} - \mathbf{R}^* : \mathbf{W}^p : \mathbf{R}^{*T} = \mathbf{W} - \mathbf{W}^c$. In terms of Euler's angles φ_1 , ϕ and φ_2 the rotation of the crystallographic lattice can be express as follows:

$$\begin{aligned} \dot{\varphi}_1 &= \Omega_{13} \frac{\sin \varphi_2}{\sin \phi} - \Omega_{23} \frac{\cos \varphi_2}{\sin \phi}, \\ \dot{\varphi}_1 &= -\Omega_{23} \cos \varphi_2 - \Omega_{13} \sin \varphi_2, \\ \dot{\varphi}_2 &= \cos \phi \left(\Omega_{13} \frac{\cos \varphi_1}{\sin \phi} - \Omega_{23} \frac{\sin \varphi_1}{\sin \phi} \right) + \Omega_{21} \end{aligned} \quad (10)$$

2.1 Continuity and co-rotation scheme

Following the arguments of Mach et al. (2010), and restricting ourselves to a viscoplastic constitutive relation, we include a non-local characteristic into the crystal plasticity model to account for the continuity condition in the lattice rotation field \mathbf{R}^* . Starting with the fundamental equation of incompatibility, $\boldsymbol{\alpha} = -\text{curl}(\mathbf{F}^{e-1})$, where $\boldsymbol{\alpha}$ is the excess dislocation density or density dislocation tensor, it is possible to demonstrate that this last expression implies that $[\mathbf{F}^{e-1}] \times \mathbf{n} = 0$, where \mathbf{n} is the vector normal to the material interface. Based in the decomposition of the deformation gradient tensor, $\mathbf{F} = \mathbf{F}^e : \mathbf{F}^p$, the previous tangential

continuity can be viewed by the inverse condition on \mathbf{F}^p , $[\mathbf{F}^p] \times \mathbf{n}_0 = 0$ where \mathbf{n}_0 is a vector normal to the interface in the reference configuration. As mentioned in the above section, in the viscoplastic case, to $\mathbf{F}^e = \mathbf{R}^*$ this condition implies that:

$$[\mathbf{F}^{e-1}] \times \mathbf{n} = 0 \Rightarrow [\mathbf{R}^{*T}] \times \mathbf{n} = 0 \Rightarrow [\mathbf{R}^{*T}] = [\mathbf{R}^*] = 0 \tag{11}$$

We can also show that

$$[\dot{\mathbf{R}}^*] = 0 \tag{12}$$

From eqs (11) and (12) we concluded that

$$[\mathbf{\Omega}] = 0 \tag{13}$$

This last equation implies that the lattice spin is continuous at the interface, and provides a constraint to be imposed to the lattice rotation field. A detailed study can be found in [Mach et al., 2010](#).

2.2 The 1-site VPSC-TGT formulation

For simulating the material response, a rate-dependent polycrystalline model is employed. In what follows, we present some features of the 1-site VPSC formulations, for a detailed description the reader is referred to [Lebensohn and Tomé \(1993\)](#). This model is based on the viscoplastic behavior of single crystals and uses a self-consistent, SC, homogenization scheme for the transition to polycrystal, VPSC. Unlike the full constraint, FC, model for which the local strains in the grains are considered to be equal to the macroscopic strain applied to the polycrystal, the SC formulation allows each grain to deform differently, according to its directional properties and depending on the strength of the interaction between the grain and its surroundings. In this sense, each grain is in turn considered as an ellipsoidal inclusion surrounded by a homogeneous effective medium, HEM, which has the average properties of the polycrystal. The interaction between the inclusion and the HEM is solved by means of the Eshelby formalism ([Mura, 1987](#)). The HEM properties are not known in advance, but they can be calculated as the average of the individual grain behaviors, once a convergence is achieved. In this paper, we will only present the main equations of the VPSC model.

The plastic strain rate \mathbf{D} in the crystal is the sum of the shear rate $\dot{\gamma}$ over all systems. The deviatoric part of the viscoplastic constitutive behavior of the material at a local level is described by means of the non-linear rate-sensitivity equation:

$$\mathbf{D} = \dot{\gamma}_0 \sum_{s=1}^{\#sys} \mathbf{m}^s \frac{\mathbf{m}^s : \mathbf{S}}{\tau_c^s} \left| \frac{\mathbf{m}^s : \mathbf{S}}{\tau_c^s} \right|^{n^s-1} = \mathbf{M} : \mathbf{S} \tag{14}$$

where \mathbf{M} is the grain visco-plastic compliance. The interaction equation, which relates the differences between the micro and the macro strain rates $(\mathbf{D}, \bar{\mathbf{D}})$ and deviatoric stresses $(\mathbf{S}, \bar{\mathbf{S}})$, can be written as follows:

$$\mathbf{D} - \bar{\mathbf{D}} = -\alpha \tilde{\mathbf{M}} : (\mathbf{S} - \bar{\mathbf{S}}) \tag{15}$$

$\tilde{\mathbf{M}}$ is the interaction tensor given by:

$$\tilde{\mathbf{M}} = (\mathbf{I} - \mathbf{S}^{esh})^{-1} : \mathbf{S}^{esh} : \bar{\mathbf{M}}, \quad (16)$$

where \mathbf{S}^{esh} is the Eshelby tensor, \mathbf{I} is the identity tensor and $\bar{\mathbf{M}}$ is the macroscopic viscoplastic compliance and α is a scalar that allows tuning the strain compatibility and stress equilibrium constraints. Its effect on the olivine LPO evolution is shown by Tommasi et al. (2000). In the present model, the standard TGT approach is used ($\alpha = 1$).

The macroscopic compliance can be adjusted iteratively using the following self-consistent equation:

$$\begin{aligned} \bar{\mathbf{M}} &= \langle \bar{\mathbf{M}} : \mathbf{B} \rangle \\ \mathbf{B} &= (\mathbf{M} + \bar{\mathbf{M}})^{-1} : (\mathbf{M} + \tilde{\mathbf{M}}) \end{aligned} \quad (17)$$

where $\langle \rangle$ denotes a weighted average over all the grains in the polycrystal and \mathbf{B} is the accommodation tensor defined for each single crystal. In addition, it is necessary to specify the evolution for the lattice orientation. The rotation rate associated with the inclusion formalism is given by:

$$\tilde{\boldsymbol{\omega}} = \boldsymbol{\Pi} : \mathbf{S}^{esh^{-1}} : (\mathbf{D} - \bar{\mathbf{D}}) \quad (18)$$

Then, the overall lattice rotation rate is given by:

$$\boldsymbol{\Omega} = \bar{\mathbf{W}} + \tilde{\boldsymbol{\omega}} - \boldsymbol{\omega}^{slip}, \quad (19)$$

where $\boldsymbol{\omega}$ is the rotation rate of the crystal lattice; $\boldsymbol{\omega}^{slip}$ is the calculated plastic rotation rate and $\bar{\mathbf{W}}$ is the applied rotation rate (screw-symmetric component of the applied velocity gradient). The grain shape updating is based on the updated deformation gradient. The square roots of the product of $\mathbf{F} : \mathbf{F}^t$ define the directions and lengths of the axes of the ellipsoid representing the grain.

The already mentioned constrains in the lattice rotation field, or continuity in $\boldsymbol{\Omega}$, is introduced in the VPSC model as a correction of the local solution of pairs of individual grains (i.e the rotation rates of each grain are derived from a 1-site calculation Eq. (19)):

$$\begin{aligned} \boldsymbol{\Omega}^1 &= \bar{\mathbf{W}} + \tilde{\boldsymbol{\omega}}^1 - \boldsymbol{\omega}^{1,slip} + \boldsymbol{\omega}^{1,cont.spin} \\ \boldsymbol{\Omega}^2 &= \bar{\mathbf{W}} + \tilde{\boldsymbol{\omega}}^2 - \boldsymbol{\omega}^{2,slip} + \boldsymbol{\omega}^{2,cont.spin} \end{aligned} \quad (20)$$

A first restriction to this additional term is $\boldsymbol{\omega}^{2,cont.spin} = -\boldsymbol{\omega}^{1,cont.spin} = \boldsymbol{\omega}^{cont.spin}$ in order to guarantee that the polycrystal average of spins fulfills the condition:

$$\begin{aligned} \boldsymbol{\omega}^1 &= \bar{\mathbf{W}} + \tilde{\boldsymbol{\omega}}^1 - \boldsymbol{\omega}^{1,slip} + \boldsymbol{\omega}^{cont.spin} \\ \boldsymbol{\omega}^2 &= \bar{\mathbf{W}} + \tilde{\boldsymbol{\omega}}^2 - \boldsymbol{\omega}^{2,slip} - \boldsymbol{\omega}^{cont.spin} \end{aligned} \quad (21)$$

The main assumption of the present scheme is coupling both fields in a very simple way. Specifically, if neighboring grains exhibit different reorientation trends, it can be expected that they will 'drag' each other. The grains or fragment of grains will spin following their own needs to fulfill contiguity:

$$\boldsymbol{\omega}^{cont.spin} = \frac{\tilde{\boldsymbol{\omega}}^2 - \tilde{\boldsymbol{\omega}}^1}{2} - \frac{\boldsymbol{\omega}^{2,slip} - \boldsymbol{\omega}^{1,slip}}{2} \quad (22)$$

Under this condition the reorientation for both grains is the same, for that reason it is named the ‘co-rotation scheme’. Eq. (22) also includes the co-rotation of the main axes of the ellipsoid.

1. Case with individual ellipsoid calculation

$$\boldsymbol{\omega}^{cont.spin} = \left(\frac{\boldsymbol{\Pi}^2 : \mathbf{S}^{2,esh^{-1}} : (\mathbf{D}^2 - \bar{\mathbf{D}}) - \boldsymbol{\Pi}^1 : \mathbf{S}^{1,esh^{-1}} : (\mathbf{D}^1 - \bar{\mathbf{D}})}{2} \right) - \frac{\boldsymbol{\omega}^{2,slip} - \boldsymbol{\omega}^{1,slip}}{2} \quad (23)$$

2. Case with average ellipsoid calculation

$$\boldsymbol{\omega}^{cont.spin} = \boldsymbol{\Pi} : \mathbf{S}^{esh^{-1}} : \left(\frac{(\mathbf{D}^2 - \bar{\mathbf{D}}) - (\mathbf{D}^1 - \bar{\mathbf{D}})}{2} \right) - \frac{\boldsymbol{\omega}^{2,slip} - \boldsymbol{\omega}^{1,slip}}{2} \quad (24)$$

Eqs. (23) or (24) assure the continuity condition of the lattice rotation field. After each incremental step of the VPSC the calculated lattice rotation field is corrected according to the last equations. This simple idea of continuity in $\boldsymbol{\Omega}$ is most probably too restrictive because, in addition to ensuring the continuity of the spin field, it implies the constancy of the misorientation between crystals. However, we believe it is an appropriate starting point for understanding the effects of such assumption.

3. RESULTS

There are several studies to simulate texture development in olivine during deformation, particularly under simple shear. As the olivine has an orthorhombic low symmetry crystal structure, it presents only a limited number of slip systems. Olivine deforms essentially by three main slip systems (010)[100], (001)[100], (010)[100] (Table 1). A challenge feature in this case is the lack of five independent slip systems at the grain scale to accommodate the imposed deformation. (010)[100] is the softest slip system and by definition we assign a critical resolved shear stress $\tau_c^{(010)[100]} = 1$. The stress exponents n_s are taken for all systems equal to 3.0. Table 1 shows the slip systems used to simulate high-temperature deformation in olivine. Higher critical resolved shear stresses are imposed on “hard” slip systems in order to close the crystal yield-loci. In this sense, we introduce additional slip systems for the purpose of having five independent systems in order to accommodate an arbitrary deformation. These deformation modes have a relative small contribution; however these artificial slip systems have a non-negligible effects in the mechanical response of the aggregate with high contrasts (Castelnau et al., 2008). In all simulations, the material is taken to be a polycrystal described by 1000 initial equiaxed grains with the same volume fraction. The strain increment per step is 1% and the convergence tolerance is set to 10^{-3} . Isotropic hardening was assumed, i.e. hardening coefficient h^s for self and latent hardening and the same. Critical stresses after finite deformation becomes a function of the accumulated total shear in the grain.

Slip System	Critical Resolved Shear Stress
(010)[100]	1.0 (reference value)
(001)[100]	1.5
(010)[001]	2.0
(100)[001]	4.0
{011}[100]	4.0
{111}[110]	50.0
{111}[011]	50.0

Table 1: Assumed potentially active slip systems and critical stresses.

3.1 Comparison to LPO interaction models

Figure 1 and Figure 2 show LPOs obtained by single shear after 0.5, 1.0, 1.5, 2.0 and 2.5 strains using classical TGT-VPSC and including continuity constraints into the lattice rotation field TGT-VPSC-CS respectively. In both cases we use the same microscopic parameters listed in Table 1. The implemented nearest-neighbor interaction scheme is independent of the linearization procedure, and can be easily transferred to another model. In all simulations the selection of the pair orientations are assigned randomly. The LPO evolution is directly related with the activated slip systems. The relative activity of the assumed slip systems are displayed in Figure 3: Evolution of the relative slip system activity in simple shear with both models: TGT-VPSC (left) and TGT-VPSC-CS (right). In both cases the “easy” slip systems accommodate more than 97% of the deformation. The others “hard” slip systems have a minor activity. The main differences arise in the relative contribution of the two softest slip systems (010)[100] and (001)[100]. The inclusion of CS constraints induce a minor participation of (010)[100] systems in favor of the (001)[100] slip systems, probably this fact is related to CS imposing constant misorientations between the pairs of interacting orientations.

The olivine LPO evolutions are not very sensitive to the relative variations of the critical resolved shear stresses of the “easy” slip systems. Many authors (Wenk et al., 1999; Tommasi et al., 2000) reported that changing the set of critical stresses by a factor of 2 or 3 they obtained similar LPO development. A common feature in both models is that once the LPO patterns were developed they remained stable. According to TGT-VPSC model as the deformation increases the LPO becomes more and more severe; in contrast with the VPSC-CS model in which the LPO show much lower intensities. In TGT-VPSC simulations the [100] and [010] axes are not parallel but display a weak asymmetric distribution relative to the maximum and minimum finite elongation directions. By including CS in the VPSC model the asymmetric distribution is clearer; in this case the LPO evolves with increasing strain to an asymmetric bimodal distribution. The two maxima have a split of approximately 30 degrees. This pattern is less clear in the [010] and [001] pole figures. The asymmetry in the pole figure can be understood in terms of the rotation of individual orientations. As the shear plane normal is approached, rotations slow down and give raise to this asymmetry. The angle of the olivine [100] maximum relative to the shear plane increases fast at low strain and more slowly at high deformation, but in any case quasi-parallelism is attained (maximum position remain stable at $\sim 10^\circ$ of the shear plane). It can be seen from Figure 3 that CS model originates a secondary maximum that shows the correct tendency (predict a stable position parallels to the shear plane).

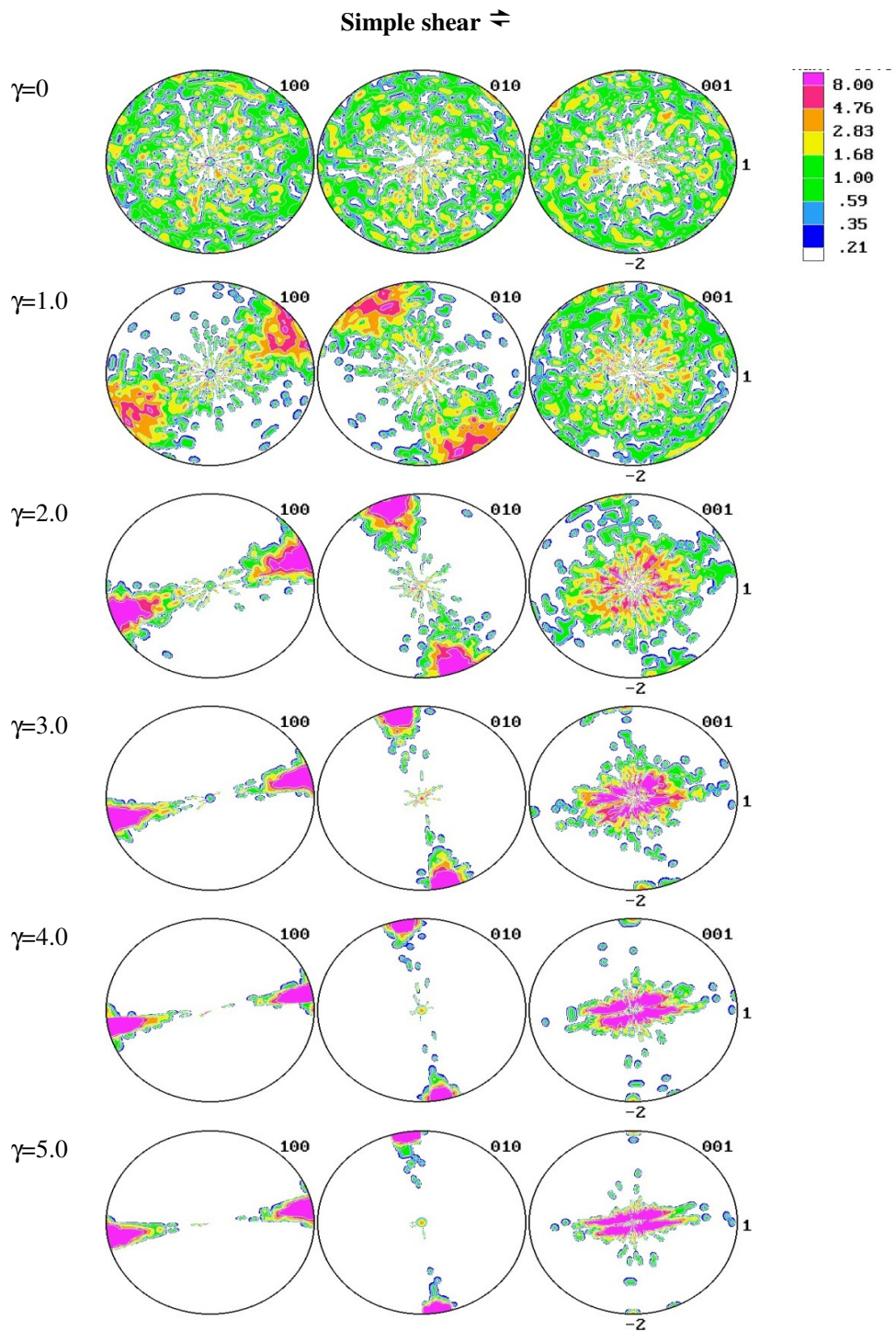


Figure 1: Olivine LPO developed in simple shear at 0, 1, 2, 3, 4, and 5 shear strains in TGT-VPSC model. Upper hemisphere equal-area projections are shown as contour levels. The shear plane is horizontal.

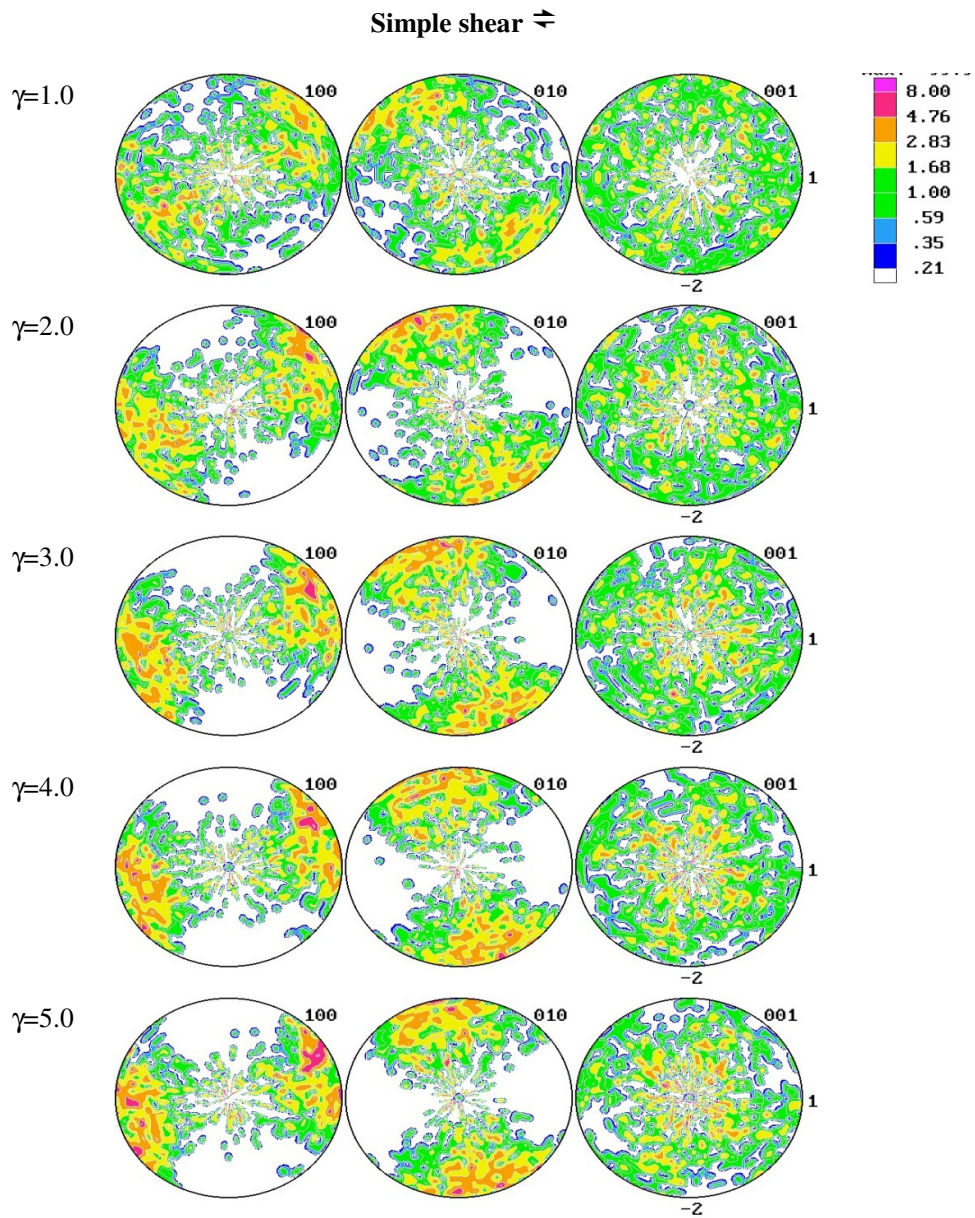


Figure 2: Olivine LPO developed in simple shear at 0, 1, 2, 3, 4, and 5 shear strains in TGT-VPSC-CS model. Upper hemisphere equal-area projections are shown as contour levels. The shear plane is horizontal.

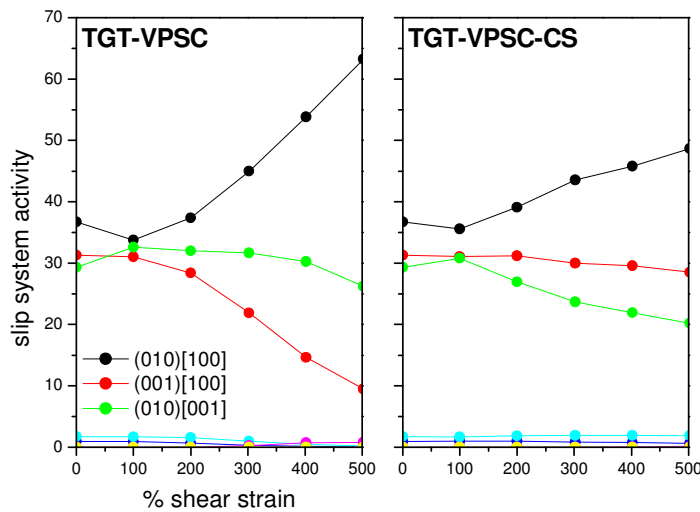


Figure 3: Evolution of the relative slip system activity in simple shear with both models: TGT-VPSC (left) and TGT-VPSC-CS (right).

3.2 LPO strength

Experimental evidence shows that the strength of texture does not increase with the increasing shear strain at large strain (Bystricky et al., 2000; Zhang and Karoto, 1995; Tommasi et al., 2000). In natural samples, J-index distribution is a Gaussian with a maximum around a value of 8 (i.e J-index square root of the integral of the square of the orientation distribution function (Bunge, 1982)). Very high texture intensities are restricted to sample with clear evidence for grain growth, while very weak textures (J-index < 4) are quite rare and limited to samples with rather small grain sizes (< 1mm) and polygonal microstructure. Models predictions always rapidly overestimate the LPO strength and the variation of the J-index with as function of the shear strain adopts value over 10 after a accumulate strain of 150% (shear strain). In all cases mentioned, the models initially have a random texture and hence the texture strength increases significantly at low strain, as expected. This rapid

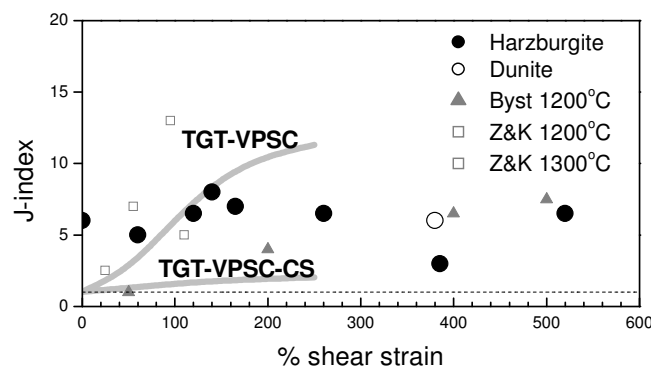


Figure 4: Evolution of J-index as function of shear strain. Dash line indicates the theoretical lower limit (J-index = 1 for a random distribution of orientation). The experimental results can be found in Tommasi et al., 2000. Comparison of the predict J-index (corresponding to [100] pole figure) for both models.

increase in the intensities in the model is showing that not all processes occurring during deformation are correctly taken into account. Also, this feature is maintained when recrystallization model is included in the VPSC simulation (Lebensohn et al., 1998; Wenk and Tomé, 1999). In **¡Error! No se encuentra el origen de la referencia.**, the predict strengths of both models are compared with experimental datasets. VPSC predicts a rapidly increasing of texture strength with the shear strain. While the inclusion of CS in the model predicts a saturation value for the J-index around 2.0, this seems to be lower than that observed experimentally (~5). However, CS model avoid the tendency to increase monotonically.

3.3 Recrystallization

Experimental measurements done by Zhang and Karato (Zhang and Karato, 1995) have shown that at large strain where recrystallization is pervasive, the texture presents the [100] parallel to the shear direction. Wenk and Tomé, (1999) shown that the [100] pattern can be adequately reproduced with VPSC in conjunction with a recrystallization model, including growth and nucleation aspects. The authors found that if nucleation dominates over growth, the model predicts stabilization for [100] maximum parallel to the shear plane in accordance with the experiments. The fact that the model predicts a good agreement assuming nucleation-dominated process can be understood through the orientations of grains that have grown. These orientations are mainly in the final stable position (i.e. parallel to the shear plane) and because they are growing at the expense of the others grains; at the end of the process only few grains, with non-negligible volume fraction, remain (see Figure 7b in Wenk and Tomé, 1999).

In the present simulations we test the selection of grain nucleation based in the crystal plastic work rate criterium. A simple approach is taken to determine whether a nucleation event took place:

$$p = \begin{cases} rnd > 0.75 & \text{if } W > \bar{W}; \text{ and } \Delta\epsilon > \epsilon_0. \\ 0 & \text{if } W < \bar{W}; \text{ or } \Delta\epsilon < \epsilon_0. \end{cases} \quad (25)$$

The nucleation probability is related with the actual work rate energy, W , and when it exceeded the polycrystalline average, \bar{W} . A random number generator (between 0 and 1) is introduced in (25) in order to distribute the nucleation events. The introduction of a second condition on the accumulated deformation, controls the possibility of multiple nucleation (i.e. before a grain nucleates it must exceed a threshold, ϵ_0 ; after first nucleation the accumulated strain increment is reset to 0, and the process starts again). If nucleation took place, like in the afore mentioned model, we use a continuous nucleation rate, where the nucleation rate is proportional to the strain rate:

$$\Delta f_{wgm} = B \mathbf{D}_{eq} f_{grain} \Delta t \quad (26)$$

f_{grain} is the current volume fraction of the grain, \mathbf{D}_{eq} is its equivalent strain-rate, and B is a constant to set the transfer size. As the nucleation events occur, the critical resolved shear stresses (CRSS) of the composite grain (parent + nucleus) are recalculated following a mix law (i.e. this scheme simplifies the fact that not the whole volume of the parent grain is associated with the new nucleus, but actually this transfer occurs in several occasions between

parent and nucleus). The nucleus does not harden and has a spherical shape. Effective CRSS and grain shape are evaluated after every strain increment:

$$\tau_{composite} = f_{nucleus} \tau_{nucleus} + (1 - f_{nucleus}) \tau_{parent} \quad (27)$$

$$axes_{composite} = f_{nucleus} axes_{nucleus} + (1 - f_{nucleus}) axes_{parent}$$

where $\tau_{nucleus}$, τ_{parent} and $axes_{nucleus}$, $axes_{parent}$ are the CRSS and grain shape of parent and nucleus regions in the composite grain, respectively. Figure 5 illustrates the general scheme of the proposed model.

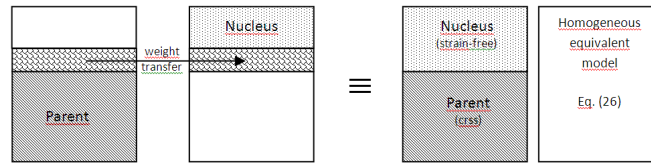


Figure 5: Schematics of the process: Each grain is divided into two parts, a parent and a nucleus volume fraction.

If nucleation occurs, weight is transferred from the parent to the nucleus volume fraction. Nucleus volume fraction increases proportional to the nucleation rate, times the time increment (see Eq.(27)).

Unlike Wenk and Tomé we use the work rate to describe the migration of the grain-boundary in the aggregate. The change of volume of a given grain is proportional to the difference between its work rate and the average (GA) or adjacent work rate (GL) depending in the selected criteria.

$$\Delta f_{growth} = C (W - \bar{W}) f_{grain}^{2/3} \Delta t \quad (GA)$$

$$\Delta f_{growth}^I = C (W^I - W^{II}) f_{grain}^{2/3} \Delta t \quad \text{if region I nucleate}$$

$$\Delta f_{growth}^{II} = -\Delta f_{growth}^I \quad (GL) \quad (28)$$

$$\Delta f_{growth}^{II} = C (W^{II} - W^I) f_{grain}^{2/3} \Delta t \quad \text{if region II nucleate}$$

$$\Delta f_{growth}^I = -\Delta f_{growth}^{II}$$

This allows some grains to grow ($W > \bar{W}$) or shrink ($W < \bar{W}$).

In what follows, we test the idea of CS constraints together with the above recrystallization model. Figure 6 and Figure 7 illustrate the model predictions for both growth criteria. The simulations are as expected: the inclusion of lattice constraint induces more realistic intensities even at large strain. In the GA case the intensities do not vary much for shear strains > 4 , whereas in GL model the intensity increases continuously related to the lack of updating of the pairs topology when any of the grains of the pairs shrink to zero volume fraction. Considering growth between adjacent grains did not introduce a significant change in the final texture.

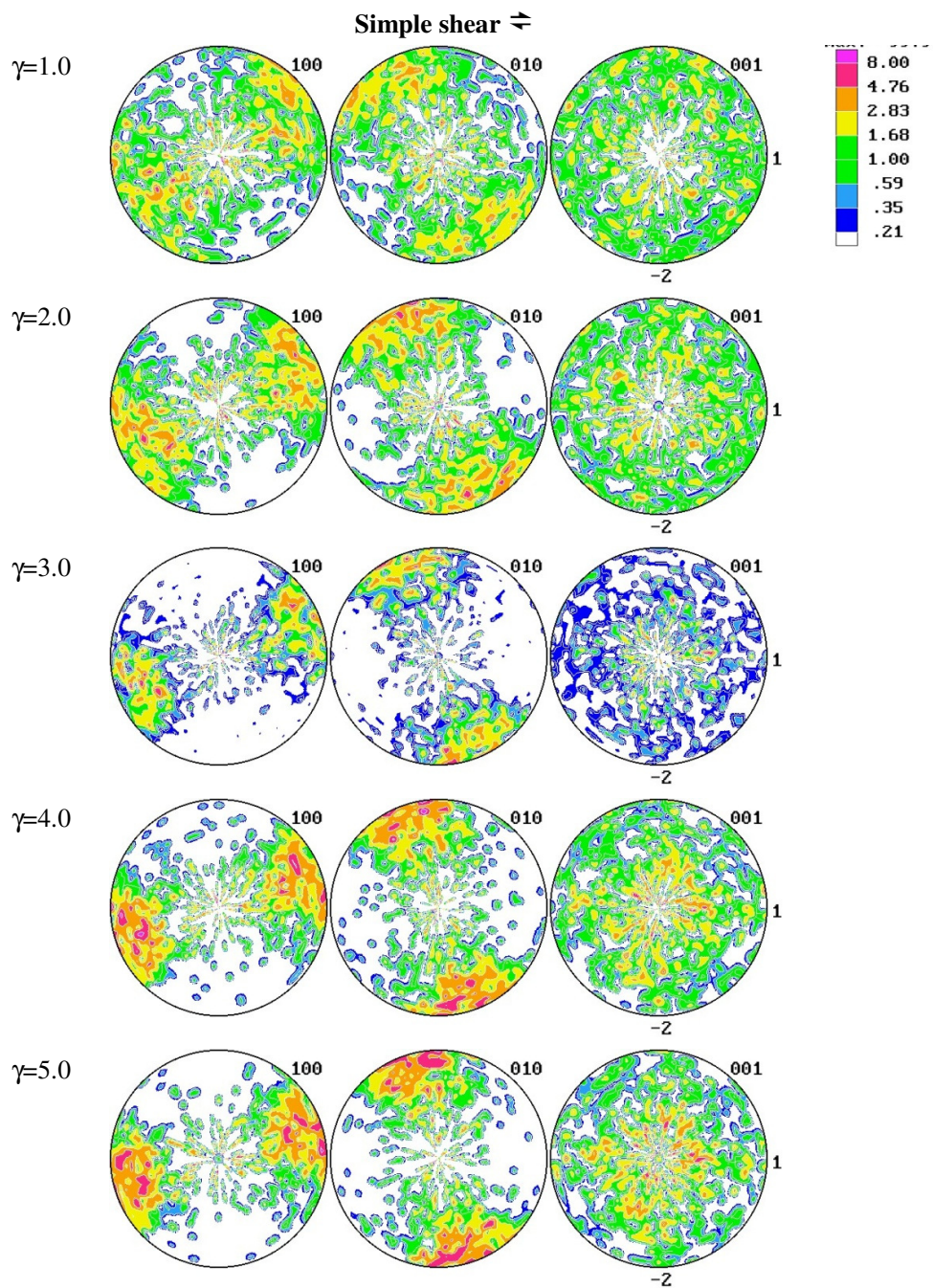


Figure 6: Texture evolution during dynamic recrystallization for the [100], [010], and [001] pole figures. The work rate of the grain is compared with the aggregate average (i.e. no microstructure topology is assumed).

Parameters: $\epsilon_0=0.4$; $B=0.75$ and $C=0.01$.

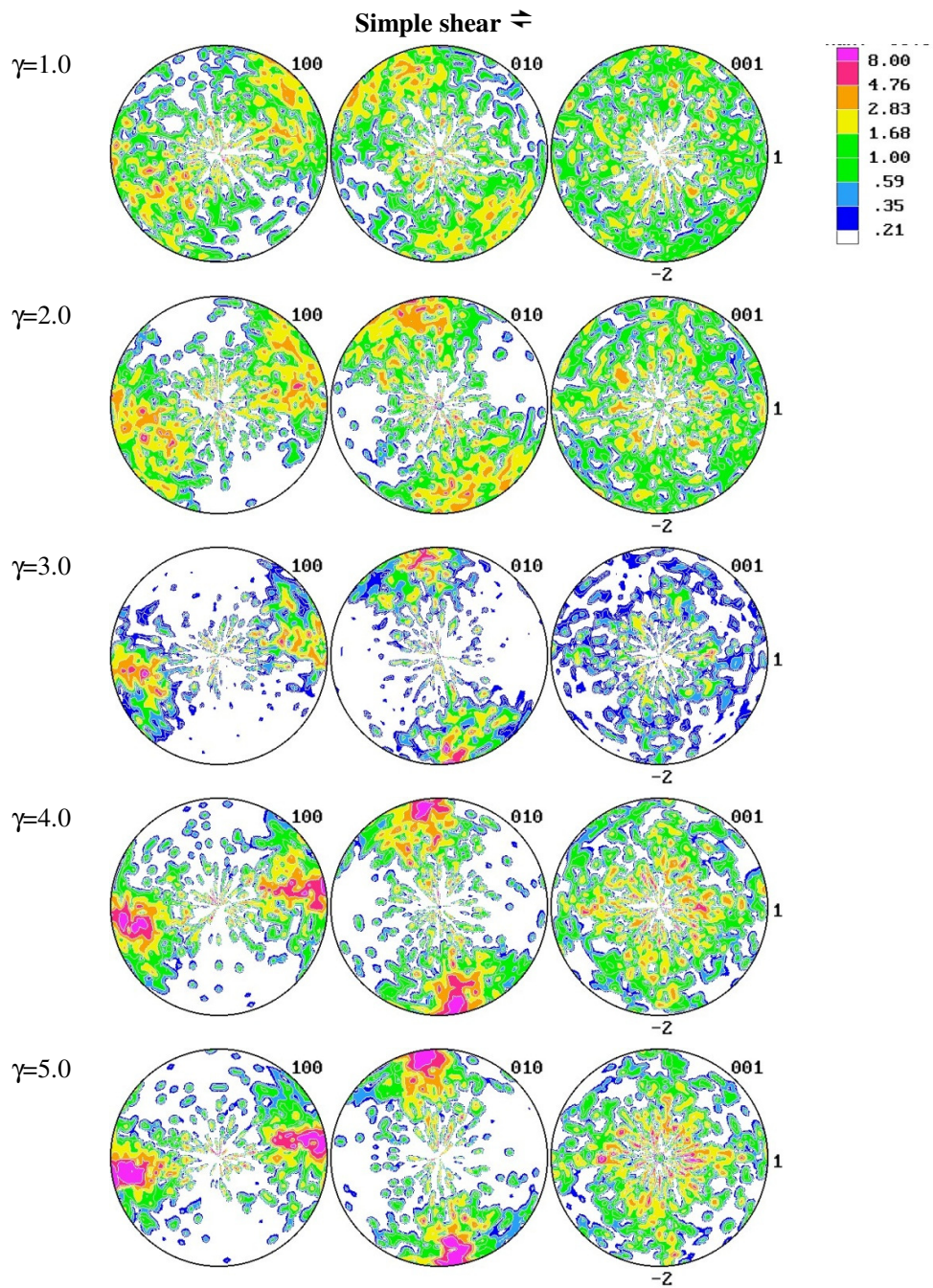


Figure 7: Texture evolution during dynamic recrystallization for the [100], [010], and [001] pole figures. The work rate of each grain is compared with the adjacent grain (i.e. the pair of co-rotating grains). Parameters: $\epsilon_0=0.4$; $B=0.75$ and $C=0.01$.

4. CONCLUSIONS

The model described in this paper should be seen as a starting point in order to obtain more realistic LPO at large strains. The model account for plastic deformation and dynamic recrystallization by subgrain rotation (nucleation) and grain-boundary migration (growth). The inclusion of an “ad hoc” continuity constraint to the lattice rotation field induces more accurate intensities at large strains. Also the model predicts a reasonable transition between a two-component texture and the tendency of grains to be parallel to the shear plane. Two criteria are analyzed to model boundary migration. The difference in strain energy is calculated between adjacent grains (i.e. the pair of co-rotating grains) and secondly with the aggregate average of the energy (i.e. no microstructure topology is assumed). Some other features could be introduced to improve the accuracy of simulation results. The inclusion of a short range interaction between pairs of adjacent grains, introducing the possibility of calculating the lattice misorientation as Fourty et al, 2010, might better control the grain boundary migration. These improvements are in progress and will be reported elsewhere.

REFERENCES

- Bai Q., Mackwell S.J., Kohlstedt D.L. High-temperature creep of olivine single crystals, 1. Mechanical results for buffered samples. *Journal of Geophysical Research*, 96:2441-2463, 1991.
- Bolmaro R.E., Fourty A., Roatta A., Bertinetti M.A., Turner P.A., Signorelli J.W. A new approach to crystal spin calculation during deformation texture development, *Scripta Materialia*, 43, Issue 6:553-559, 2000.
- Bolmaro R.E., Fourty A., Signorelli J.W., Brockmeier H.G., Development of wire drawing textures in Cu-Fe: the influence of macroscopic and microscopic heterogeneities. *Modelling and Simulation in Materials Science and Engineering* 14, 1-19, 2006.
- Bunge H.J. *Texture analysis in materials sciences*, Butterworths, 1982.
- Bystricky M., Kunze K., Burlini L., Burg J.-P. High shear strain of olivine aggregates: rheological and seismic consequences, *Science*, 290:1564-1567, 2000.
- Castelnau O., Blackman D.K., Lebensohn R.A., Ponte Castañeda P. Micromechanical modeling of the viscoplastic behavior of olivine, *Journal of Geophysical Research*, 113:1-18, 2008.
- Chastel Y.B., Dawson P.R., Wenk H.R., Bennett K. Anisotropic convection with implications for the upper mantle, *Journal of Geophysical Research*, 98:17757-17771, 1993.
- Fourty A., Signorelli J.W., Bolmaro R.E. Continuidad del campo de rotación en materiales FCC. Estudio de su influencia en el desarrollo de texturas de laminado, *Presente Congreso*, 2010.
- Hutchinson M.M., Pascoe R.T. Grain-boundary strengthening in copper-base solid solutions, *Metal Science Journal*, 6:90-95, 1972.
- Kaminski É., Ribe N.M., Browaeys J.T. D-Rex, a program for calculation of seismic anisotropy due to crystal lattice preferred orientation in the convective upper mantle, *Geophysical Journal International*, 158:744-752, 2004.
- Lebensohn R.A., Tomé C.N. A self-consistent anisotropic approach for the simulation of plastic deformation and texture development of polycrystals: Application to zirconium alloys, *Acta Metallurgica et Materialia*, 41, Issue 9:2611-2624, 1993.
- Lebensohn R.A., Wenk H.-R., Tomé C. N. Modelling deformation and recrystallization textures in calcite, *Acta Materialia*, 46, Issue 8:2683-2693, 1998.
- Mach J., Beaudoin A., Acharya A. Continuity in the plastic strain rate and its influence on texture evolution, *Journal of Mechanics and Physics of Solids*, 58, Issue 2: 105-128, 2010.

- Mainprice D., Silver P.G. Interpretation of SKS-waves using samples from the subcontinental lithosphere, *Physics of the Earth and Planetary Interiors*, 78, Issues 3-4:257-280, 1993.
- Mura T. *Micromechanics of defects in solids*, Martinus Nijhoff Publishers, 1987.
- Ribe N.M., Yu Y. A theory of plastic deformation and textural evolution of olivine polycrystals, *Journal of Geophysical Research*, 96:8325-8335, 1991.
- Signorelli J.W., Turner P.A., Sordi V., Ferrante M., Vieira, E.A., Bolmaro R.E., Computation modeling of texture and microstructure evolution in Al alloys deformed by ECAE. *Scripta Materialia* 55, 1099-1102, 2006.
- Simo J., Vu-Quoc L. Three dimensional finite strain rod model. Part II: Computational aspects, *Electronics Research Laboratory Memorandum*, No. UCB/ERL M85/31, 1985.
- Thorsteinsson T. Fabric development with nearest-neighbor interaction and dynamic recrystallization, *Journal of Geophysical Research Solid Earth*, 107:2014-2026, 2002.
- Tomé C.N., Lebensohn R.A., Necker C.T., Mechanical anisotropy and grain interaction in recrystallized aluminium. *Metallurgical and Materials Transactions A* 33A, 2365-2648, 2002.
- Tommasi A., Mainprice D., Canova G., Chastel Y. Viscoplastic self-consistent and equilibrium-based modelling of olivine lattice preferred orientations. 1. Implications for the upper mantle seismic anisotropy, *Journal of Geophysical Research*, 105:7893-7908, 2000.
- Wenk H.R. and Tomé C.N. Modelling dynamic recrystallization of olivine aggregates deformed in simple shear, *Journal of Geophysical Research*, 104:25513-25527, 1999.
- Wenk H.R., Bennett K., Canova G.R., Molinari A. Modeling plastic deformation of peridotite with the self-consistent theory, *Journal of Geophysical Research*, 96:8337-8349, 1991.
- Zhang S. and Karato S.-I. Lattice preferred orientation of olivine deformed in simple shear, *Nature*, 375:774-777, 1995.
- Zhang S., Karato S.-I., Fitz Gerald J., Faul U.H., Zhou Y. Simple shear deformation of olivine aggregates, *Tectonophysics*, 316, Issues 1-2:133-152, 2000.